Template Synthesis of Hollow Metal Oxide Fibers with Hierarchical Architecture

Rusheng Yuan, Xianzhi Fu,* Xinchen Wang, Ping Liu, Ling Wu, Yiming Xu, Xuxu Wang, and Zhanyi Wang

Research Institute of Photocatalysis, College of Chemistry & Chemical Engineering, Fuzhou University, Fuzhou 350002, People's Republic of China

Received April 28, 2006. Revised Manuscript Received July 24, 2006

Hollow metal oxide fibers (TiO_2 and Fe_2O_3) have been prepared by using activated carbon fibers (ACFs) as the templates, through a simple impregnation and heat treatment. The resulting products, as compared to ACFs, possessed not only a similar morphological feature upward to the micrometer scale but also different surface nanostructures with unique morphology. The TiO_2 fibers displayed overlapped "wormlike" surface and a hierarchical structure with two distinguishable layers, the inner layer and the outer layer, which were composed of the particles of 7 and 15 nm, respectively. It was also found that the reaction temperature had a significant effect on the TiO_2 surface morphology. The Fe_2O_3 fibers exhibited a rough and crinkle-like surface and were also composed of hierarchical particles. Both TiO_2 and Fe_2O_3 fibers possessed the hierarchical pore structure with mesopores in the walls of the large hollow channel. Such porous architecture favored the resultant TiO_2 with better apparent photoactivity than P25 titania for degradation of gaseous acetone and would also make the materials useful for further application in other fields.

1. Introduction

Metal oxides have many important applications such as in heterogeneous catalysis,[1] solar cells,[2,3] sensors,[4] and optical-electric devices.[5,6] The performances of metal oxides depend not only on their chemical compositions and surface properties but also greatly on their textural properties including morphology, surface area, pore volume, and pore dimension. Great effort thus has been dedicated to the metal oxide synthesis with a controllable morphology and pore-wall structure. One of the important approaches is template-directing synthesis. Biomaterials,[7−10] latex/silica nanoparticles,[11] porous alumina,[12] polymer gel,[13] and surfactant[14] have been largely used as the template, which can be easily removed from the hybrid material through dissolution in an appropriate solvent or via combustion.

Recently, there have been increasing interests in the introduction of nanoscaled substructure into the metal oxides. The synthesized metal oxides possess an interconnected pore network with controlled porosity on several length scales.[15−17] Such hierarchical porous materials are of particular interest in the catalysis and separation process, because of the improved diffusion of guest species through the network of pores and channels. In general, two or more templates are combined to build up these complexes. For example, Kuang et al.[15] used polystyrene, block copolymer, and an ionic liquid as templates to prepare a trimodal porous silica. Smått and co-workers[16] used a versatile double-templating route to synthesize a bimodal porous silica monolith. On the other hand, the bimodal porous oxide can be made by using a single chemical template, for instance, surfactant.[17] However, few studies have been done using a single physical template to fabricate the hierarchical oxides. Such a process is simple and also much easier to control the morphology of the final product than the system with two or more templates.

Over the past few years many groups have used carbon materials as a template for oxide synthesis.[18−21] In the present study, we have examined activated carbon fiber (ACF) as a physical template for the synthesis of hollow metal oxide fibers (TiO_2 and Fe_2O_3). ACF has a high specific surface area, a high adsorption rate and capacity, and a relatively

* To whom correspondence should be addressed. E-mail: xzfu@fzu.edu.cn. Fax: +86-591-83738608.

(1) Pirkanniemi, K.; Sillanpää, M. *Chemosphere* **2002**, *48*, 1047.
(2) Rossinyol, E.; Arbiol, J.; Peiró, F.; Cornet, A.; Morante, J. R.; Tianb, B.; Bob, T.; Zhao, D. *Sens. Actuators, B* **2005**, *109*, 57.
(3) Palomares, E.; Clifford, J. N.; Haque, S. A.; Lutz, T.; Durrant, J. R. *J. Am. Chem. Soc.* **2003**, *125*, 475.
(4) Graf, M.; Barrettino, D.; Taschini, S.; Hagleitner, C.; Hierlemann, A.; Baltes, H. *Anal. Chem.* **2004**, *76*, 4437.
(5) Malik, A.; Sêco A.; Fortunato, E.; Martins, R. *J. Non-Cryst. Solids* **1998**, *227−230*, 1092.
(6) Umadevi, P.; Nagendra, C.L. *Sens. Actuators A* **2002**, *96*, 114.
(7) Davis, S. A.; Burkett, S. L.; Mendelson, N. H.; Mann S. *Nature* **1997**, 385.
(8) Huang, J.; Kunitake, T. *J. Am. Chem. Soc.* **2003**, *125*, 11834.
(9) Caruso, R. A.; Schattka, J. H. *Adv. Mater.* **2000**, *12*, 1921.
(10) Imai, H.; Matsuta, M.; Shimizu, K.; Hirashima, H.; Negishi, N. *J. Mater. Chem.* **2000**, *10*, 2005.
(11) Velev, O. D.; Kaler, E. W. *Adv. Mater.* **2000**, *12*, 531.
(12) Yanagishita, T.; Nishio, K.; Masuda, H. *Adv. Mater.* **2005**, *17*, 2241.
(13) Shchukin, D. G.; Schattka, J. H.; Antonietti, M.; Caruso, R. A. *J. Phys. Chem. B* **2003**, *107*, 952.
(14) Peng, T.; Hasegawa, A.; Qiu, J.; Hirao, K. *Chem. Mater.* **2003**, *15*, 2011.
(15) Kuang, D.; Brezesinski, T.; Smarsly, B. *J. Am. Chem. Soc.* **2004**, *126*, 10534.
(16) Smått, J.-H.; Schunk, S.; Lindén, M. *Chem. Mater.* **2003**, *15*, 2354.
(17) Wang, X.; Yu, J. C.; Ho, C.; Hou, Y.; Fu, X. *Langmuir* **2005**, *21*, 2552.
(18) Schüth, F. *Angew. Chem., Int. Ed.* **2003**, *42*, 3604.
(19) Tao, Y.; Kanoh, H.; Kaneko K. *J. Am. Chem. Soc.* **2003**, *125*, 6044.
(20) Bottini, M.; Tautz, L.; Huynh, H.; Monosov, E.; Bottini, N.; Dawson, M. I.; Bellucci, S.; Mustelin, T. *Chem. Commun.* **2005**, *8*, 758.
(21) Lee, S.; Sigmund, W. M. *Chem. Commun.* **2003**, *6*, 780.

10.1021/cm0609911 CCC: $33.50
Published on Web 08/18/2006

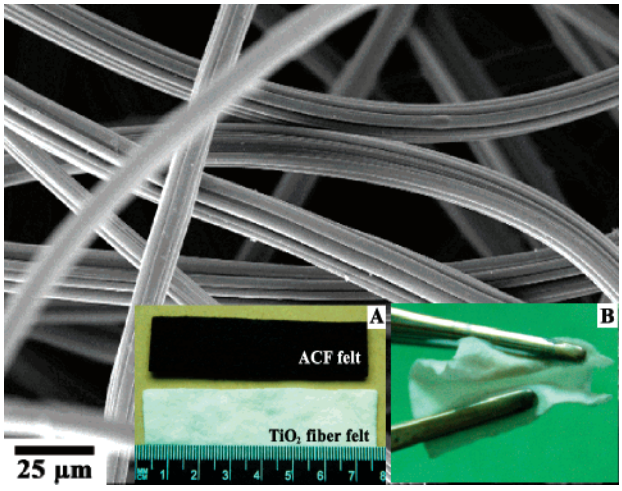

Figure 1. SEM image of ACFs. The inset A shows the photograph of the ACF felt and the final TiO_2-180 fiber felt. The inset B exhibits that the TiO_2 fiber felt possesses rather good strength and toughness and can be handled easily without breaking up into fine powder.

uniform pore size in the micropore range.[22] The Wakayama group[23] has employed activated carbon (fibers, granules, and powders) as the template for synthesis of porous TiO_2 and SiO_2 through the supercritical fluids process. This process replicates faithfully not only the macroscopic shapes but also the porous structures on a nanometer scale, and the resulting solid fiber has a diameter of 7 μm. Different from them, the negative copy (hollow TiO_2 and Fe_2O_3 fibers) as opposed to a true replication was produced by a simple and relatively mild method when ACF was used as the template. The process to incorporate the inorganic material within ACFs was performed by impregnation and heat treatment under autogenous pressure, both of which are simple processes and can be carried out readily without strict requirement for experimental conditions. More significantly, the final products not only inherit the structural characteristics of ACF templates on the micrometer scale but also possess the unique hierarchical microstructures, obviously different from the parent template. In addition, the photocatalytic activity of TiO_2, a typical photocatalyst, was determined by degradation of acetone in the gas medium.

2. Experimental Section

2.1. Materials. The ACF sample used in this work was produced from rayon precursor, in the form of felt (the black part in the inset A of Figure 1). It has a BET surface area of 749 m^2/g and a micropore size with a sharp maximum at about 0.67 nm. The fibers were pretreated with concentrated nitric acid (65%) for 12 h to remove the surface impurities and create the oxygenated functionalities. After washing with distilled water, the fiber was dried at 110 °C in air for 6 h. Titanium tetraisopropoxide (TTIP; 99%) and iron(III)−acetylacetonate (99%) were purchased from Shanghai Reagent Corporation. All other reagents (analytical grade) were purchased from Beijing Chemical Plant and used without further purification.

2.2. Synthesis of Hollow Metal Oxide Fibers. The hollow TiO_2 fibers were synthesized as follows. Typically, 1 g of the acid-treated ACF was immersed into 175 mL of solution containing TTIP and anhydrous ethanol at a volume ratio of 1:6. After sonicating for 0.5 h, the filled ACF together with the solution was transferred to a stainless steel autoclave and heated at a certain temperature (150, 170, 180, or 210 °C) for 24 h. When it was cooled down to room temperature, the sample was taken out and rinsed with anhydrous ethanol to remove the excess of TTIP between the fibers and then dried at 60 °C. Finally, the composite fibers of all samples were calcined at the same temperature of 600 °C (ramp of 5 °C/min) in a flow of O_2 (60 mL/min) for 5 h, respectively. This procedure ensured the complete removal of ACF template and the formation of TiO_2 crystalline, as confirmed by thermogravimetric analysis (TGA). The resulting sample of hollow TiO_2 fibers is denoted as TiO_2-*T*, where *T* is the temperature employed for the hydrolysis reaction of precursors (TTIP) in the autoclave. For synthesis of TiO_2 fibers, all of the reacted precursors (TTIP) were completely converted into the hollow TiO_2 fibers without producing other forms of TiO_2. A similar procedure was employed to synthesize the hollow Fe_2O_3 fibers by using iron(III)−acetylacetonate as the precursor and anhydrous acetone as the solvent, and the autoclave temperature was set at 180 °C.

2.3. Characterization. Scanning electron microscopy (SEM) measurements were carried out on a JEOL JSM-6700F instrument operated at 5 kV. Transmission electron microscopy (TEM) images were taken on a JEOL JEM-2010EX instrument operated at 200 kV. The X-ray diffraction (XRD) patterns were recorded on a Bruker D8 Advance X-ray diffractometer using Cu Kα irradiation, and the scanning speed was 2° (2θ)/min in the range of 10−80°. The BET surface area was determined via N_2 adsorption at 77 K on a Micromeritics ASAP 2000. Before the measurements, all samples were degassed at a temperature of 250 °C for 6 h. The pore size distribution was calculated by the method of density functional theory. TGA was performed on a Netzsch STA409PC thermal analysis instrument, with a heating rate of 10 °C/min from 30 to 900 °C under an oxygen atmosphere.

2.4. Photocatalytic Studies. The photocatalytic activity of the prepared TiO_2-180 fibers was determined through the degradation of gaseous acetone in a 2500 mL glass container. The container was connected to a quartz reactor surrounded with four 8-W UV lamps (with major emission at 365 nm) and interfaced to a gas chromatograph (GC, Hewlett-Packard 4890). A closed circulation reaction system, including the container, the reactor, and the GC, was established with the aid of a circulation pump.

A total of 0.12 g of the catalyst was packed into the quartz reactor with an inner size of 15 × 15 × 2 mm. Prior to the photodegradation experiments, the catalyst was allowed to reach a steady state with acetone in the dark for 4 h, and the equilibrium concentration of acetone was 460 ppm. The flow rate of the system was 20 mL/min, and the reaction temperature was controlled at 32 ± 1 °C by an air-cooling system. The concentrations of residual acetone and the produced CO_2 were measured at an interval of 30 min by gas chromatography, equipped with a Porapak R column, a flame ionization detector, and a thermal conductivity detector. For comparison, the photocatalytic activity of commercial TiO_2, Degussa P25, was also tested under the same reaction conditions and with the equal catalyst weight as those employed for TiO_2-180.

3. Results and Discussion

Hollow TiO_2 Fibers. As shown in Figure 1, the parent ACF has an average diameter of 16 μm. The surface is not smooth and displays several linear grooves and ridges aligned

(22) Cloirec, P. L.; Subrenat, E. *Energy Fuels* **1997**, *11*, 331.
(23) Wakayama, H.; Itahara, H.; Tatsuda, N.; Inagaki, S.; Fukushima, Y. *Chem. Mater.* **2001**, *13*, 2392. Fukushima, Y.; Wakayama, H. *J. Phys. Chem. B* **1999**, *103*, 3062. Tatsuda, N.; Fukushima, Y.; Wakayama, H. *Chem. Mater.* **2004**, *16*, 1799.

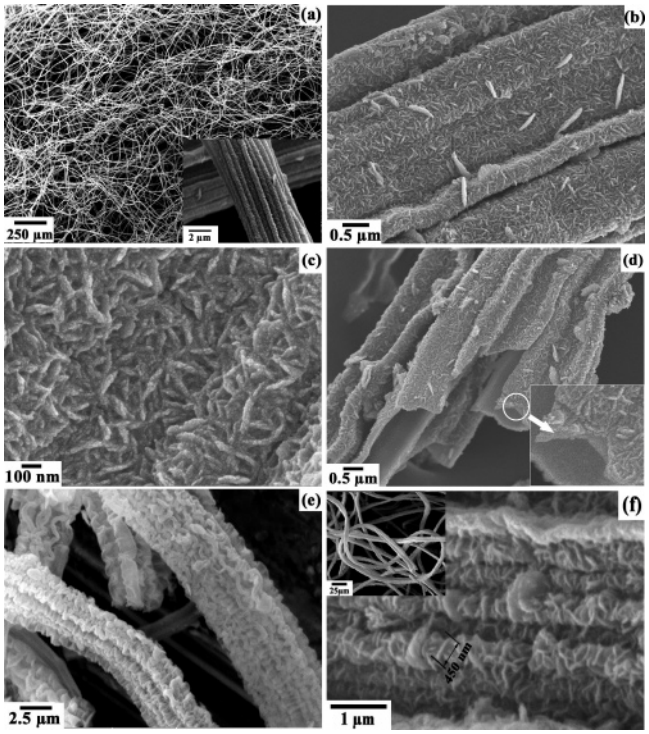

Figure 2. SEM images of hollow TiO_2 fibers: (a) overview of the titanium dioxide replica (inset, the single fiber at a higher magnification), (b and c) higher magnification showing the surface worm-like structure, (d) a broken TiO_2 fiber indicating the hollow nature (the inset is the enlarged pattern of the region marked with a circle), and (e and f) the resultant TiO_2 fibers with crinkle structure when titanium precursors were attached to ACF templates at 150 and 170 °C.

in the longitudinal direction. This is due to the surface oxidation that occurred during the process of ACF synthesis.[24] As a result of the strong adsorption of ACF, the precursor molecules were quickly adsorbed and reacted with the functional groups (especially hydroxyl) on the fiber surface and water molecules subsequently generated from condensation reaction. This leads to the tight anchor of the molecules on the host fiber surface, forming a uniform guest coating. Upon calcination, the ACF template was removed, giving rise to the self-supporting TiO_2 textile.

The TiO_2-180 textile (the white part in the inset A of Figure 1) retained the morphological characteristics of the original fiber felt except for some shrinkage (about 20%) in size due to calcination. As shown in Figure 2a, the TiO_2-180 textile was composed of TiO_2 fibers with a large length on the centimeter scale. The different magnifications of individual TiO_2 fibers (Figure 2b,c) showed that the ridge structure of the original fiber was faithfully replicated. However, the fiber surface was covered uniformly with many overlapped "worm-like" structures of TiO_2, which rendered the macroscopic textile full of externally irregular interspaces. From the broken section of the TiO_2 fiber (Figure 2d), it could be seen that the TiO_2 fiber was hollow, with a uniform wall thickness of about 250 nm. Because the diameter of the template fiber was much larger than the wall thickness of the hollow TiO_2 fiber, the hollow structure collapsed partly during the calcination, making the outer diameter of the fiber

(24) Brasquet, C.; Rousseau, B.; Estrade-Szwarckopf, H.; Cloirec, P. L. *Carbon* **2000**, *38*, 407.

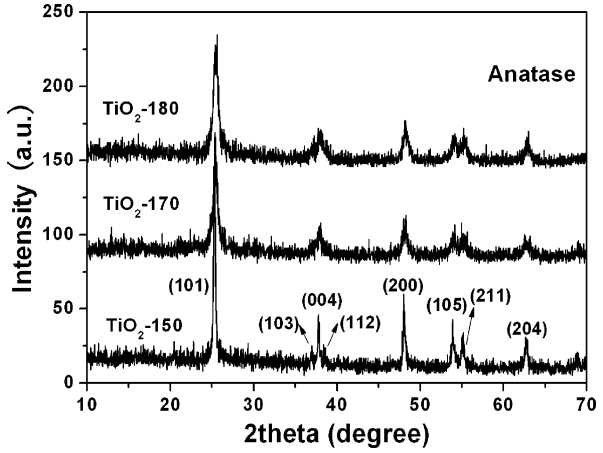

Figure 3. XRD patterns of the resulting TiO_2 fibers when titanium precursors were attached to ACF at 150, 170, and 180 °C.

shrink to about 5 μm. The wide-angle XRD pattern of TiO_2-180 (Figure 3) indicated that the TiO_2 particles constructing the hollow fibers were in the anatase phase. Moreover, the XRD results revealed that the higher temperature of the hydrolysis reaction favored the formation of smaller particles in the samples. This might be attributed to that the higher reaction temperature may accelerate hydrolysis of the precursors and produce a more crystalline nucleus, leading to the formation of a larger number of the crystalline particles with smaller size during the subsequent calcination process.

The hollow nature of TiO_2 fibers was also confirmed by TEM, as shown in Figure 4a. The micrographs of high magnification TEM (Figure 4b,c) revealed that the TiO_2 fiber consisted of two kinds of uniform particles, with average diameters of about 15 and 7 nm, respectively. The crystalline sizes of titania in the TEM images were consistent with the average crystalline size of 10 nm estimated from the XRD results (Figure 3). The fiber wall exhibited the hierarchical and lamellar structure, as marked with the short arrow in the inset of Figure 2d. The particles on the fiber inner layer were small and close-packed, forming a relative smooth surface, whereas the outer layer was made up of larger particles and took on an overlapped worm-like structure. The presence of bimodal particle sizes in the TiO_2 fibers may be ascribed to the interaction between ACF and amorphous titania. As the amorphous titania resided in the inner layer interacted strongly with ACF, the crystal growth of titania during post calcination was greatly suppressed, leading to the formation of smaller particles. In the case of the outer layer, the interaction of amorphous titania with ACF was relatively weak and resulted in the formation of bigger particles. The similar explanation may also be applied to the Fe_2O_3 fibers.

Although the TiO_2-180 was calcined at 600 °C for 5 h, it still has a BET surface area of 79 m^2/g. This can be regarded as the result of the hollow nature as well as the mesoporous structure of the fiber wall (Figure 5). As compared to the ACF template, TiO_2-180 fibers displayed a wider pore size distribution with a main peak at ~3.3 nm, indicating mesoporosity of the fibers. Part of the pores with a typical wormhole-like structure in the inner layer of the fiber wall was clearly discernible (Figure 4b,c, the insets with an arrow). Both of the pores located in the wall and the

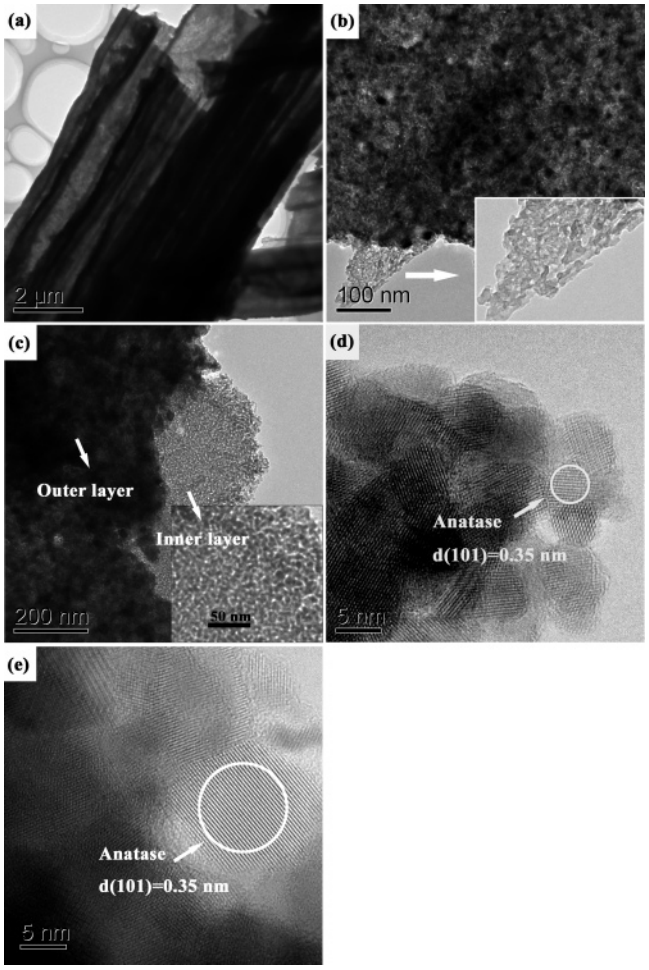

Figure 4. TEM images of TiO_2-180 fibers: (a) the hollow feature at low resolution, (b and c) the different particles composing the fiber wall, and (d and e) high-resolution TEM images of inner and outer layer of TiO_2 fiber, respectively. The lattice fringes corresponding to anatase TiO_2 are clearly observed.

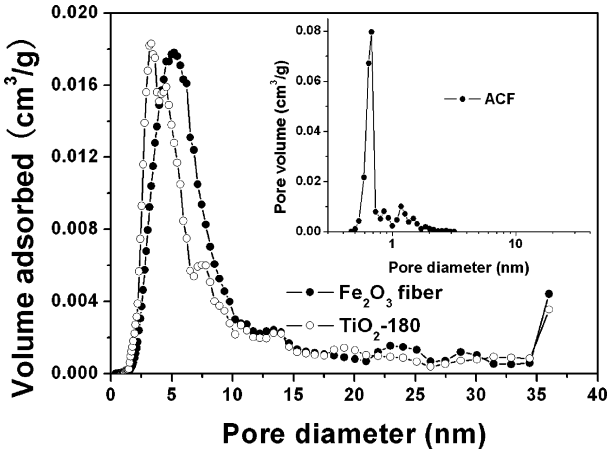

Figure 5. Pore size distributions of TiO_2-180 fibers, Fe_2O_3 fibers, and ACF templates (shown in the inset).

macroscopically hollow channels are made up of constituted hierarchical pore structure. The lattice spacing (0.35 nm), obtained from the high-resolution TEM images (Figure 4d,e), was in good agreement with that estimated from the XRD pattern of the anatase phase.

The attachment of titanium precursors to ACF was also performed at 150 and 170 °C in an autoclave, followed by the same calcination procedure as that for TiO_2-180. The

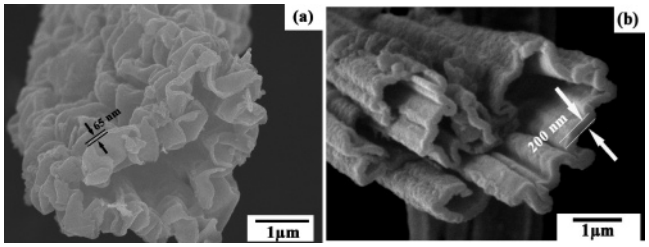

Figure 6. SEM images of (a) TiO_2-150 fiber and (b) TiO_2-170 fiber.

as-synthesized products, TiO_2-150 and TiO_2-170, exhibited almost the same structure as TiO_2-180 on a macroscopic scale. All of the XRD peaks for the both samples (Figure 3) can be assigned to a pure phase of anatase TiO_2. However, there were some differences in the surface morphology (Figure 2e,f). The surface of the TiO_2-150 fiber was full of crinkle-like structure, different from that of TiO_2-180. This can be ascribed to the fact that the wall of the fiber is flimsy and smooth and easy to curl and shrink during the sintering process. Comparatively, the TiO_2-170 fiber showed a rough surface, which was constructed by randomly oriented TiO_2 flakes with a length of 450 nm. This was different from the interconnected worm-like unit with small dimension observed from TiO_2-180. Meanwhile, the wall thicknesses of TiO_2-150, TiO_2-170 (Figure 6), and TiO_2-180 were about 65, 200, and 250 nm, respectively. The corresponding BET surface areas for the samples were 48, 67, and 79 m^2/g. Thus, it can be concluded that the temperature at which the hydrolysis reaction of titanium precursors was conducted had a significant effect on the surface morphology, wall thickness, and surface area of the resultant hollow TiO_2 fibers.

The effect of temperature on the morphology of hollow TiO_2 fiber gives some indication of the reaction mechanism. Under the anhydrous conditions, the titanium precursor molecules first reacted with the functional groups (especially hydroxyl) on the fiber surface via a ligand exchange,[25] leading to a generation of isopropanol. As the temperature increased, the condensation of isopropanol was accelerated and produced more water molecules, which were further reacted with the precursors in situ, resulting in the fiber with a thicker wall and worm-like substructure. When the temperature was higher than 200 °C, the hydrolysis reaction was too fast to form TiO_2 fibers, leading to the formation of many large agglomerations. Therefore, control of surface morphology and wall thickness of the TiO_2 hollow fiber could be easily achieved by changing the reaction temperature.

Hollow Fe_2O_3 Fibers. Similar replication could be made for other metal oxides such as ferric oxide. TiO_2 was formed by the surface sol−gel process,[8] which is based on adsorption of TTIP from solution onto the hydroxylated surface of ACF and the subsequent hydrolysis reaction. Unlike TTIP, iron(III)−acetylacetonate molecules are stable in aqueous media and undergo a pyrolysis process by heating, leading to formation of Fe_2O_3.[26] The iron precursors were first adsorbed on ACFs, forming a compact coating layer during the heat treatment under autogenous pressure. The small compact-packed particles are distributed uniformly on the surface of

(25) Ichinose, I.; Kawakami, T.; Kunitake, T. *Adv. Mater.* **1998**, *10*, 535.
(26) Pal, B.; Sharon, M. *Thin Solid Films* **2000**, *379*, 83.

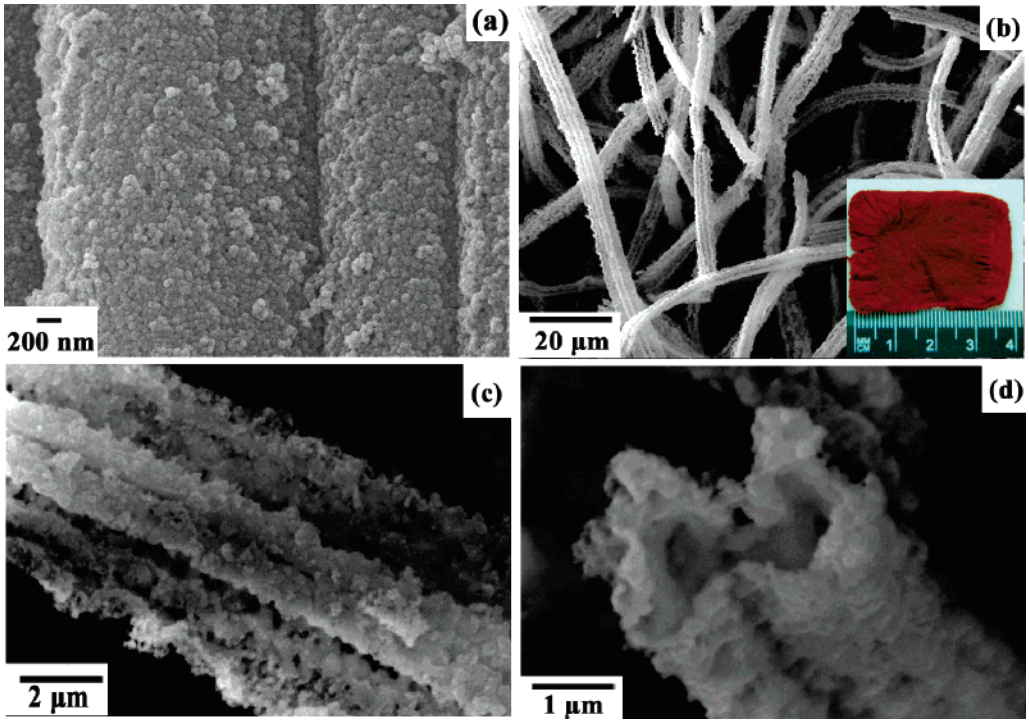

Figure 7. SEM images of (a) the formed coating when iron precursors were attached to ACF during heat treatment under autogenous pressure, (b) overview of the Fe_2O_3 fibers (part of the fibers is broken because the sample was crushed during the process of sampling), (b) surface structure of an individual fiber at a higher magnification, and (c) section of the fiber presenting the hollow interior. Inset of part b: photograph of the synthesized Fe_2O_3 textile.

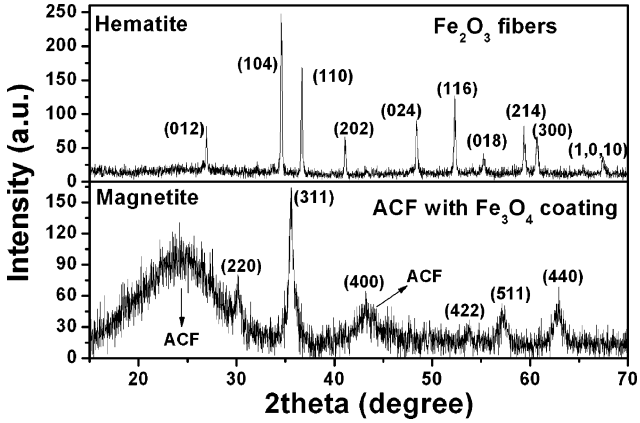

Figure 8. XRD patterns of the resulting Fe_2O_3 fibers and the unfired ACF with the Fe_3O_4 coating derived from iron precursors.

the ACF, as shown in Figure 7a. However, XRD analysis (Figure 8) demonstrated that the formed particles of iron oxide before calcination were the crystallites of Fe_3O_4, instead of Fe_2O_3. This can be ascribed to the fact that part of the Fe(III) species is reduced into Fe(II) by the ACF template during the heat treatment. It has been reported that the surface functional groups impart a reduction ability to ACF that can reduce metal ions such as Pt(IV), Pd(II), Ag-(I), and Au(III) ions into a lower valence ion or metallic elements.[27−29] In this regard, this method also provides an alternative route to synthesize the coating of Fe_3O_4 nanoparticles.

After the sample was calcined in the O_2 atmosphere, the ACF templates were removed, and meanwhile Fe_3O_4 was oxidized, resulting in the brownish-red Fe_2O_3 fibers (Figure 7b). The fibers replicated the ridge structure and large length of the original fibers but with a very rough and crinkle-like surface, which was covered with many aggregates of particles irregularly. The diameter of hollow Fe_2O_3 fiber shrank to about 6.5 μm, due to the calcination. The wall thickness was thin and uneven, and some surface macropores connected with the inner hollow channel (Figure 7c,d). TEM and high-resolution TEM images (Figure 9) showed that the Fe_2O_3 fibers, like the TiO_2 fibers, were also made up of two kinds of particles, with an average diameter of 9 and 25 nm, respectively. But the lamellar structure was not obvious. The XRD pattern (Figure 8) indicated that all the diffraction peaks could be indexed as the α-Fe_2O_3 phase. It should be noted

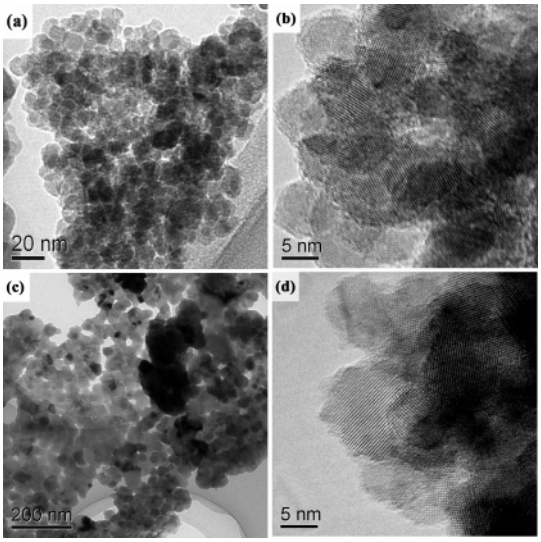

Figure 9. Particles from the Fe_2O_3 fiber wall: (a and c) TEM images and (b and d) high-resolution TEM images.

(27) Chen, S.; Zeng, H. *Carbon* **2003**, *41*, 1265.
(28) Uchida, M.; Shinohara, O.; Ito, S.; Kawasaki, N.; Nakamura, T.; Tanada, S. *J. Colloid Interface Sci.* **2000**, *224*, 347.
(29) Fu, R.; Zeng, H.; Lu, Y. *Carbon* **1993**, *31*, 1089.

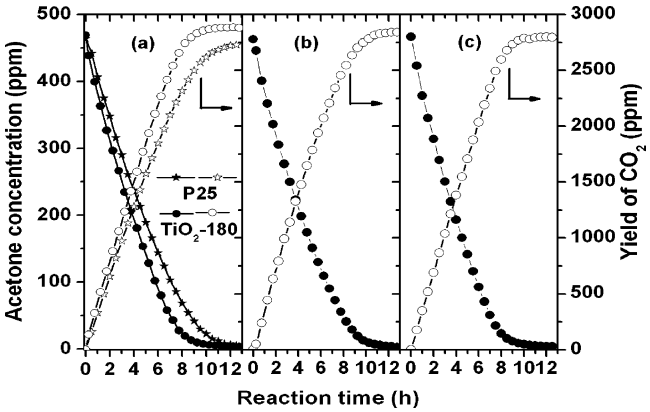

Figure 10. Concentration change of acetone and yield of CO_2 with time under UV irradiation: (a) the first cycle; (b) the second cycle; and (c) the third cycle.

that the average crystalline size of Fe_2O_3 (46 nm) estimated from the XRD results (Figure 8) was about twice as large as the size of the bigger particles in the TEM images (Figure 9). This discrepancy might be ascribed to the formation of twin-crystal-like particles, which could be observed clearly in Figure 9. The BET surface area of hollow Fe_2O_3 fibers was 98 m^2/g, slightly higher than that of TiO_2 fibers. The pore size distribution of Fe_2O_3 fibers (Figure 5) was similar to that of TiO_2 fibers, probably due to the same ACF templates used. ACF has highly slit-shaped micropores on the external surface,[22] and part of precursor molecules can enter into the pores and form the reverse copy after removal of the template. Thus, the porous structure of the template was passing onto the inner layer of the resultant fiber wall. These interconnected pore networks should allow light transport and molecule accessibility to the active site during the photocatalytic reactions or other kinds of heterogeneous catalysis. Therefore, we tested the photocatalytic performance of TiO_2, a widely used photocatalyst for environmental purification.

Photocatalytic Activity. The photocatalytic activities of the as-prepared TiO_2-180 fibers and the referenced P25 were examined for the decomposition of gaseous acetone (Figure 10). It can be seen that the anatase TiO_2-180 exhibited better performance than the P25, the highly photoactive rutile−anatase composite. The acetone molecules were efficiently mineralized, as demonstrated by CO_2 formation. It should be pointed out that, even with the same equilibrium concentration for TiO_2-180 and P25 when the reaction began, the actual initial concentration of acetone for the former was larger than that for the latter because a larger amount of acetone molecules was adsorbed by the former with a larger surface area, thus causing the final yield of CO_2 by TiO_2-180 higher than that by P25. The better photocatalytic performance of the obtained TiO_2-180 can be mainly attributed to the larger accessible surface area and the structural properties. Generally, a larger surface area can offer more adsorption and reaction sites for reactants, and the hierarchical pore network favors diffusion of the reactant molecules into the catalyst. In addition, the smaller crystal size is also beneficial to enhance photocatalytic activity of TiO_2-180. Therefore, the proposed synthesis route produced hollow TiO_2 fibers with better apparent photoactivity than P25.

The cyclic performance of TiO_2-180 was also tested. Before the next run, the products of the last run were released, and gaseous acetone was injected repeatedly into the reactor until a steady concentration of 460 ppm was reached. From Figure 10, it was observed that TiO_2-180 at the second and third run presented similar photocatalytic behaviors as the first run, indicating that the activity of TiO_2-180 was stable. Furthermore, TiO_2 in the form of textile on the centimeter scale is inherently preferable for handling during practical applications compared to nanosized particles.

4. Conclusions

This work has developed a simple and effective method for fabrication of hollow TiO_2 and Fe_2O_3 fibers by using ACFs as the template. The synthesized products were in the form of textile composed of fibers on the centimeter scale, inherited from the parent template. Moreover, the novel hierarchical structures of morphology and porosity were successfully built up. These structural features endowed the prepared TiO_2-180 with better photocatalytic performance for decomposition of gaseous acetone than P25. Also, such a porous nature, plus the textile form, renders the materials interesting for solar energy, optoelectronic devices, and catalyst support. ACF is a kind of ideal and universal template for various purposes, because it can anchor fast to the precursor molecules on its surface by physical adsorption, whether the chemical reaction between them exists or not. This fact, along with the simplicity of the proposed method, provides the possibility to synthesize other materials with similar nanostructures.

Acknowledgment. This work was financially supported by the National Natural Science Foundation of China (Nos. 20373011, 20473017, 20573020, and 20537010) and the National Key Basic Research Special Foundation of China (No. 2004CCA07100). X.C.W. thanks the *Ming River Scholars* program of Fujian province, P. R. China.

CM0609911